Letter

Kohn-Sham-Proca equations for ultrafast exciton dynamics

J. K. Dewhurst
Max-Planck-Institut fur Mikrostrukturphysik, Weinberg 2, D-06120 Halle, Germany

D. Gill and S. Shallcross
Max-Born-Institute for Non-linear Optics and Short Pulse Spectroscopy, Max-Born Strasse 2A, 12489 Berlin, Germany

S. Sharma*
Max-Born-Institute for Non-linear Optics and Short Pulse Spectroscopy, Max-Born Strasse 2A, 12489 Berlin, Germany and Institute for Theoretical Solid-State Physics, Freie Universität Berlin, Arnimallee 14, 14195 Berlin, Germany

(Received 30 January 2024; accepted 17 January 2025; published 6 February 2025)

A longstanding problem in time-dependent density functional theory has been the absence of a functional able to capture excitonic physics under laser pump conditions. Here we introduce a scheme of coupled Kohn-Sham and Proca equations in a pump-probe setup that we show (i) produces linear-response excitonic effects in the weak pump regime in excellent agreement with experiment, but also (ii) captures excitonic physics in the highly nonlinear regime of ultrafast strong laser pumping. In particular "bleaching" (i.e., reduction) of the excitonic weight and the appearance of excitonic side bands is demonstrated. The approach is a procedural functional—the Kohn-Sham and Proca equations are simultaneously time propagated—allowing the straightforward inclusion of, for example, lattice and spin degrees of freedom into excitonic physics. The functional is shown to have universal applicability to a wide range of materials, and we also establish a relation between the parameters used in the functional and the exciton Bohr radii of the materials.

DOI: 10.1103/PhysRevB.111.L060302

Introduction. Spintronics, magnonics, valleytronics, and excitonics [1,2] are all potential alternatives to conventional charge-based electronics, which are reaching their limits both in component and power densities. In all of these fields, laser light is used to modulate and control the fundamental excitations of a material to generate spin, valley, or exciton current [3,4]. With a view towards the next generation of optoelectronic devices, the field of transient opto-*excitonics*, i.e., the ultrafast laser-induced creation, dynamics, and control of exciton dynamics, is one of the most promising [5–7].

A fully *ab initio* method to describe such physics of light-matter interaction is time-dependent density functional theory (TD-DFT) [8]: it has already proved its strength in the fields of spin- and valleytronics, predicting new phenomena as well as providing a full microscopic understanding of the physics [9–16]. So far, however, the approximations used in TD-DFT are unable to describe the time-dependent spectra of laser-pumped excitons in solids. In contrast, for the linear-response regime (i.e., when the light perturbation is very weak), TD-DFT has proved very successful in computing the excitonic spectra of diverse materials [17–20]. Following this approach, TD-DFT can be rewritten as a Dyson equation linking the Kohn-Sham noninteracting particle response to the full material response via the exchange-correlation (xc) kernel, $f_{\rm xc}(\mathbf{r},\mathbf{r}',t-t')\equiv\delta v_{\rm xc}(\mathbf{r}t)/\delta\rho(\mathbf{r}'t')$, where $v_{\rm xc}$ is the exchange-correlation potential and ρ is the electronic charge density. To describe excitons in solids, this xc kernel in the $q\to 0$ limit (i.e., for long-wavelength pulses) must go as $f_{\rm xc}\to 1/q^2$ [21,22]. On this basis, several approximate xc kernels have been designed that successfully describe the excitonic response of real materials [17–20]. However, since these approximations are exclusively in the form of xc kernels, their use is restricted to a linear regime and cannot be extended to strong-field pumped time-dependent excitons. It is thus, at present, not possible to have a unified method that can treat linear and strong-field excitons and, most importantly, it is not possible to study excitronics (the dynamics of pumped excitons) using the most prominent method of choice, TD-DFT.

In this work, we describe a real-time TD-DFT method for solids that captures the dynamics of excitons by coupling the electronic Kohn-Sham (KS) equations to an effective vector potential $\mathbf{A}_{\rm xc}$, which is time dependent but not spatially varying. We show that $\mathbf{A}_{\rm xc}$ as a solution of a *Proca equation*, which is the Maxwell equation containing a mass term, generates the functional for $\mathbf{A}_{\rm xc}$ that correctly describes the excitonic response in the linear as well as strong-field regimes. We demonstrate this by theoretical arguments as well as by numerical results; by comparison with experiment, we demonstrate that in the weak pump-probe regime, the

*Contact author: sharma@mbi-berlin.de

Kohn-Sham-Proca (KSP) functional correctly gives the linear-response limit and also good agreement with experiments for the dynamics of a strongly pumped exciton.

Method. Real-time TD-DFT [8,23] rigorously maps the computationally intractable problem of interacting electrons to a KS system of noninteracting electrons in an effective potential. The time-dependent KS equation is

$$i\frac{\partial\psi_j(\mathbf{r},t)}{\partial t}=\left(\frac{1}{2}\left\{-i\nabla-\frac{1}{c}[\mathbf{A}(t)+\mathbf{A}_{\rm xc}(t)]\right\}^2+v_s(\mathbf{r},t)\right)\times\psi_j(\mathbf{r},t), \tag{1}$$

where ψ_j is a KS spinor orbital and the effective KS potential $v_s(\mathbf{r},t)\equiv v(\mathbf{r},t)+v_{\rm H}(\mathbf{r},t)+v_{\rm xc}(\mathbf{r},t)$ consists of the external potential v, the classical electrostatic Hartree potential $v_{\rm H}$, and the exchange-correlation (xc) potential $v_{\rm xc}$. The vector potential $\mathbf{A}(t)$ represents the applied laser field within the dipole approximation (i.e., the spatial dependence of the vector potential is absent) and $\mathbf{A}_{\rm xc}(t)$ is the xc vector potential. Note that unless otherwise stated, atomic units are used throughout.

Within TD-DFT, two conceptual routes exist to calculate the response in solids: (a) linear-response formalism and (b) real-time TD-DFT. The former case is valid for very weak perturbation where the TD-DFT equation can be cast into a Dyson-like equation to determine the response, requiring $f_{\rm xc}\to 1/q^2$ as $q\to 0$ for the xc kernel [17,18,20,23]. It is important to note that in this case, the xc kernel is a_2/q^2, where the scaling $a_2<1$ for weak and $a_2>1$ for strongly bound excitons (see Ref. 14 in Ref. [20]).

Looking at this, one would imagine that since $f_{\rm xc}(\mathbf{r},\mathbf{r}',t-t')\equiv\delta v_{\rm xc}(\mathbf{r}t)/\delta\rho(\mathbf{r}'t')$, one could choose a corresponding form for $v_{\rm xc}$ to describe excitons in the latter form of TD-DFT, i.e., real-time TD-DFT. However, this assumption is invalid at a practical level for periodic solids—excitons cannot be treated by merely improving the lattice-periodic $v_{\rm xc}$ since the $q\to 0$ limit has already been taken. Any part of the response which is finite in this limit is necessarily excluded.

This problem can, however, be solved in the following manner: the crucial quantity appearing in the response formalism is $V(\mathbf{q})\chi_s(\mathbf{q})$, where $\chi_s(\mathbf{q})$ is the KS response function. In the $q\to 0$ limit, this becomes an indeterminate form and can be replaced by an expectation value of the momentum operator $\hat{\mathbf{p}}=-i\nabla$. Emulating this with a lattice-periodic calculation thus requires coupling to the variable conjugate to $\hat{\mathbf{p}}$, namely, the xc vector potential $\mathbf{A}_{\rm xc}(t)$ [24–26]. It follows that within TD-DFT, excitons and their dynamics can be described by the time dependence of the total current. The procedure for determining the optical response then is to solve the time-dependent Hamiltonian with $\mathbf{A}_{\rm xc}(t)$ and, using the KS orbitals obtained as a solution to this Hamiltonian, evaluating the total current $\mathbf{J}(t)$, which itself is obtained by integrating the current density $\mathbf{j}(\mathbf{r},t)$ in the unit cell [27]. This gauge-invariant current density is given by

$$\mathbf{j}(\mathbf{r},t)={\rm Im}\sum_j^{\rm occ}\psi_j^\dagger(\mathbf{r},t)\nabla\psi_j(\mathbf{r},t)-\frac{1}{c}[\mathbf{A}(t)+\mathbf{A}_{\rm xc}(t)]\rho(\mathbf{r},t). \tag{2}$$

The Fourier transform of this current to frequency space is used to generate the optical conductivity $\sigma(\omega)$, via the linear-response equation $\mathbf{J}(\omega)=\sigma(\omega)\mathbf{E}(\omega)$, where $\mathbf{E}(t)=-(1/c)\,\partial\mathbf{A}(t)/\partial t$ is the physical (or external) electric field. This conductivity is then used to obtain the dielectric function [28], $\varepsilon(\omega)=1+4\pi i\sigma(\omega)/\omega$. Since the full current is used to obtain the response, local field effects are automatically included [27].

One still requires an explicit functional form for $\mathbf{A}_{\rm xc}$ capable of capturing the excitonic response of real solids. All approximate exchange-correlation functional forms are ultimately choices, often based on heuristic arguments. In our case, the physical vector potential of electromagnetism obeys Maxwell's equation, and so a natural guess might be to obtain $\mathbf{A}_{\rm xc}$ as the solution of a Maxwell-like equation. This was recently implemented and tested by Sun *et al.* [26]. This approach, however, results in an uncontrolled divergence of the time-dependent current.

Why does the coupled TD-DFT Maxwell approach of Sun *et al.* diverge? The reason for this is not any essential divergence of the coupled Kohn-Sham-Maxwell equations approach: this method has been successfully used before for finite systems [29]. In this case, the electromagnetic field radiates energy away from the center and, consequently, acts as a dissipative system [29]. However, in the case of periodic boundary conditions with a spatially independent vector potential, all unit cells, and hence the entire system, behave coherently. The vector potential $\mathbf{A}(t)$ feeds back into the TD-DFT equations to increase the current, which itself enhances the vector potential via the Maxwell equation, and so on, resulting in a numerically unstable procedure.

This can be demonstrated. We first examine the solutions of the massless Maxwell equation and, as a first step, look at the simplest case with no current term $J(t)$, i.e., the "free solution." This yields, for the Maxwell equation, a solution of the form $A_{\rm xc}(t)=c_0+c_1t$ and, for the Proca equation, $A_{\rm xc}(t)=c_1\sin(\sqrt{a_0/a_2}\,t+c_0)$. Strikingly, the solution of the Maxwell equation diverges, while that of the Proca equation oscillates at frequency $\omega=\sqrt{a_0/a_2}$. As a second step, one can then choose a simplistic form for $J(t)$, such as a Gaussian [Fig. 1(a)], to study the solution for a full nonhomogeneous equation. This is shown in Fig. 1(b) from which it is clear that the features of the free solution are inherited by the full nonhomogeneous equations; the solution of the Maxwell equation diverges, while that of the Proca equation oscillates with frequency proportional to the ratio $\sqrt{a_0/a_2}$.

In a realistic case, this current $\mathbf{J}(t)$, rather than being fixed, arises as the solution of Kohn-Sham equations coupled to, and simultaneously propagated with, the Maxwell or Proca equation. As demonstrated in Fig. 1(c) for the case of LiF, the current—as well as $\mathbf{A}_{\rm xc}$—diverges for the Maxwell equation, which cannot be cured by any scaling of the xc potential $v_{\rm xc}$, but can be delayed in time. This delay allows for a short window in which a response can be determined and was done in the work of Sun *et al.* However, this makes the procedure invalid for the study of real-time laser-pumped excitons. The Proca equation solution, on the other hand, remains finite and oscillatory. All calculations in this work are performed using the state-of-the-art full-potential linearized augmented plane-wave method [30] as implemented in the ELK code

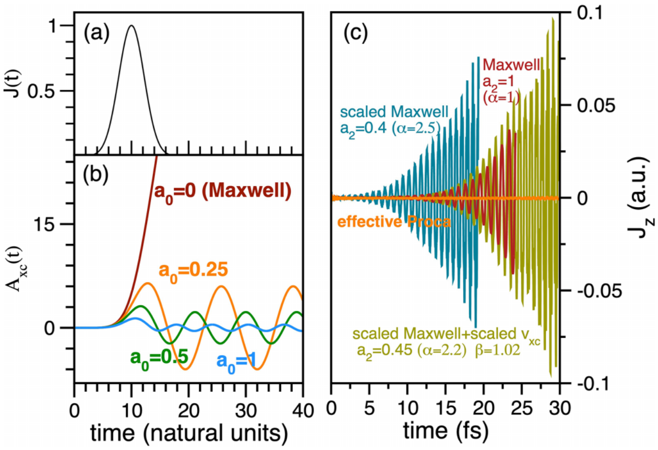

FIG. 1. (a) Current $\mathbf{J}(t)$. (b) $\mathbf{A}_{\rm xc}(t)$ obtained by solving the Proca [see Eq. (3)] and Maxwell equations [obtained by setting $a_0 = 0$ and $a_2 = 1$ in Eq. (3)] with $\mathbf{J}(t)$ from (a). (c) $\mathbf{A}_{\rm xc}(t)$ for LiF obtained by solving coupled Eqs. (2) and (3). For all values of a_2, as well as for scaling of the xc potential $\beta v_{\rm xc}$ as suggested in Ref. [26], the current diverges when the Kohn-Sham system is coupled to an effective Maxwell equation. In contrast, for the Kohn-Sham-Proca scheme ($a_0 = 0.25$), the current remains finite and oscillatory at all times.

[31,32]. We have used the local density approximation for the exchange-correlation functional (for further details, see the Supplemental Material [33]).

Can we nevertheless improve on this functional generated via the Maxwell equation to make it both stable and have wide applicability? For this, we look at a more general form of the Maxwell equation itself, namely, the so-called Proca equation that includes a mass term and which, in the absence of spatial variations, is

$$a_2\frac{\partial^2}{\partial t^2}\mathbf{A}_{\rm xc}(t) + a_0\mathbf{A}_{\rm xc}(t) = \frac{4\pi c}{\Omega}\mathbf{J}(t), \tag{3}$$

where a_0 and a_2 are parameters (the Maxwell equation is obtained by setting $a_2 = 1$ and $a_0 = 0$), and Ω is the unit-cell volume. Note the prefactor of c in Eq. (3): this along with the prefactor of $1/c$ in Eq. (2) ensures that the effects generated by $\mathbf{A}_{\rm xc}$ are *nonrelativistic* in nature. This is analogous to the xc magnetic field $\mathbf{B}_{\rm xc}$, arising from interactions between electrons, rather than being relativistic in origin.

Thus we propose a functional form for $\mathbf{A}_{\rm xc}$ by coupling TD-DFT to an effective Proca equation. It should be stressed that while the Proca equation entails that the xc field is massive, this should not be interpreted as a physical mass but rather an effective field, the aim of which is to reproduce the time-dependent current.

This type of functional is *procedural* in that $\mathbf{A}_{\rm xc}$ is determined not from a simple formula, but rather by the procedure of computing the instantaneous $\mathbf{J}(t)$ from the KS wave function at each time step and using this current to advance the Proca equation (3) to the next time step. Since the Proca equation is a second-order differential equation, two initial values are required. As $\mathbf{A}_{\rm xc}$ describes the response of the electron system to the external electromagnetic field, it is natural to choose $\mathbf{A}_{\rm xc}(0) = \dot{\mathbf{A}}_{\rm xc}(0) = 0$. If we convert $\mathbf{A}_{\rm xc}$ into its electric field form, $\mathbf{E}_{\rm xc}(t) = -(1/c)\,\partial\mathbf{A}_{\rm xc}(t)/\partial t$, we find this satisfies

$$a_2\frac{\partial}{\partial t}\mathbf{E}_{\rm xc}(t) + a_0\int_0^t dt'\,\mathbf{E}_{\rm xc}(t') = -\frac{4\pi}{\Omega}\mathbf{J}(t), \tag{4}$$

from which $v_{\rm xc}(\mathbf{r}, t) = -\mathbf{E}_{\rm xc}(t)\cdot\mathbf{r}$ would be the corresponding scalar potential, which is clearly not lattice periodic. Once again, we can see from the lack of factors of c that this exchange-correlation potential is nonrelativistic in origin. It is interesting to note that this a rare example of a functional specific to TD-DFT, instead of a ground-state functional used adiabatically. In fact, it has no effect on the ground state because there the total current is zero. Furthermore, it has memory effects because it does not exclusively depend upon the instantaneous $\mathbf{J}(t)$, but also upon its own state.

It is not sufficient for an approximate functional to be stable. It must also exhibit *universality*; in other words, it should be predictive for a wide range of materials, including hypothetical examples, while being free of adjustable parameters. As we will see below, the Proca functional satisfies this condition since the parameters a_0 and a_2 can be determined for any given material merely from its band gap. Furthermore, one can ascribe physical meaning to the parameters used in the Proca equation. To do this, let us suppose that spatial variations are also included in the Proca equation. In the static limit, this becomes $\nabla^2 v_{\rm xc} = (1/\lambda^2)v_{\rm xc}$, where $\lambda = \sqrt{a_2/a_0}$, the solution of which is the Yukawa potential $v_{\rm xc}(r) = (1/r)\exp(-r/\lambda)$. Thus, λ provides a natural length scale for the functional which, as we will demonstrate, is proportional to the excitonic Bohr radius. In the work of Sun *et al.* [26], a_0 is implicitly zero and thus their solutions correspond to weakly bound excitons of infinite extent.

It should be noted that this form of the Proca equation can be further generalized by adding a term proportional to the first derivative of the vector potential: $a_1\partial\mathbf{A}_{\rm xc}(t)/\partial t$. This acts as a dissipative term and would serve to decrease the lifetime of the exciton, which would be useful in very long time simulations. As an ultimate generalization, the parameters a_0, a_1, and a_2 could also be made into 3×3 matrices accounting for directional inhomogeneity in the materials.

In the present work, we simulate a realistic experimental pump-probe setup; $\mathbf{J}(\omega)$ is obtained by taking the difference between the currents obtained from two calculations—one with the pump pulse alone and one with both pump and probe pulses. We associate the time delay between the pump and the probe pulses with the time at which the material is probed after pumping.

Excitonic physics in weak pump pulse regime. We now explore the performance of the coupled KSP equations as applied to study materials under pump-probe conditions. We first study the case of a weak pump pulse of duration of 12 fs with the material being probed 50 fs after pumping. The pump and the probe pulses are kept to the same low fluence of 0.001 mJ/cm^2.

Presented in Fig. 2, for 10 different materials [47–49], is the absorption [i.e., the imaginary part of the dielectric function $\varepsilon(\omega)$] calculated using the KSP pump-probe scheme, using the random phase approximation (RPA) within linear-response formalism of TD-DFT (i.e., by solving the Dyson equation) and experimental linear-response

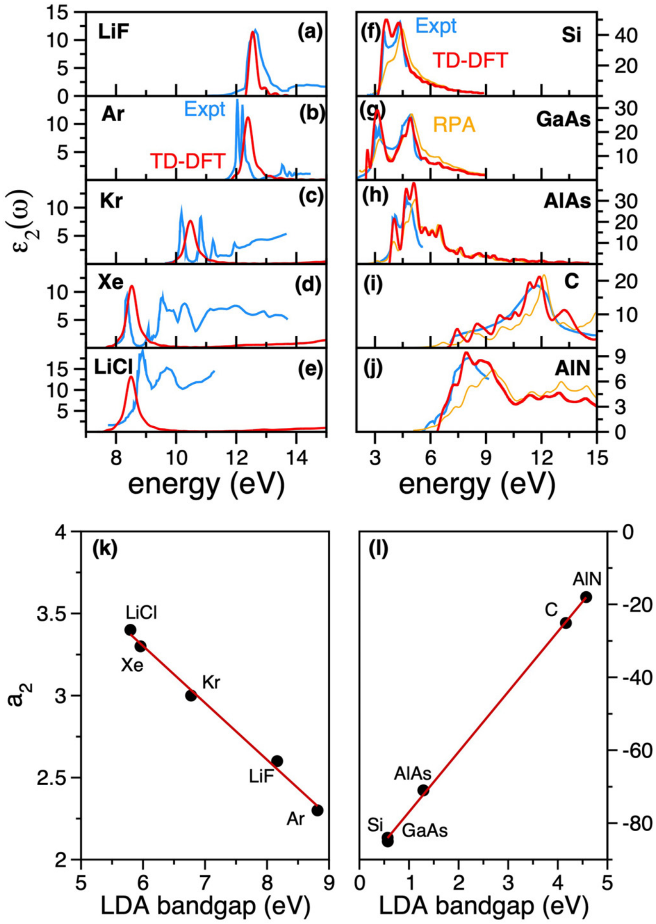

FIG. 2. Imaginary part of the dielectric tensor, $\varepsilon_2(\omega)$, as a function of photon energy (in eV) for (a)–(e) strongly bound and (f)–(j) weakly bound excitonic materials. Experimental data are taken from the following sources: LiF [34], Ar [35], Kr [36], Xe [35], LiCl [37], Si [38], GaAs [39], AlAs [40], C [41], and AlN [42] (see Table I of the Supplemental Material [33] for details), with random phase approximation (orange) results also shown for comparison. Variation of the a_2 parameter as a function of the Kohn-Sham band gap (in eV) for (k) strongly bound excitonic and (l) weakly bound excitonic materials. The red line is the fit to the data.

absorption spectra. The wide-gap insulators [Figs. 2(a)–2(e)] all exhibit strongly bound exciton resonances with binding energies ranging from 0.94 to 1.7 eV, and the KSP procedural functional is seen to provide excellent agreement for the main excitonic peak position and its height. For noble gas solids [Figs. 2(b)–2(d)], the KSP scheme well captures the main exciton, but not the excited states of the exciton (i.e., the Rydberg series). In the case of LiCl [Fig. 2(e)], calculations are performed for an ideal crystal structure while experiments are performed for thin films grown on LiF, leading to disagreement at above-band-gap energies. For the semiconductors [Figs. 2(f)–2(j)], excitonic physics shows up instead as a pronounced lowering and redistribution of the spectral weight as compared to RPA, and here once again the KSP scheme is seen to yield excellent agreement with the experimental linear-response spectra. Overall, we thus conclude that the KSP procedural functional in a pump-probe scheme captures very well the excitonic physics, correctly reproducing the linear-response regime in the weak pumping limit.

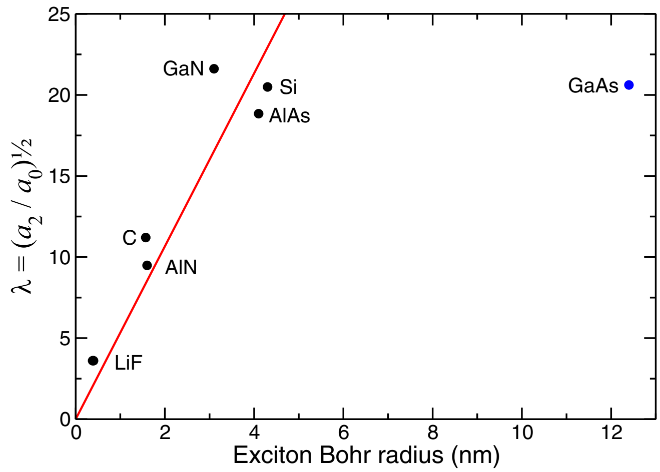

FIG. 3. Plot of exciton Bohr radius vs length scale of the $\mathbf{A}_{\rm xc}$ functional given by $\lambda = \sqrt{a_2/a_0}$. The radii are obtained from Ref. [43], and references therein, and Refs. [44–46]. The line is a fit to the data (excluding the GaAs point) and passing through zero.

Universal form for the proca equation. In obtaining these results, the KSP procedure involved two material-dependent parameters, a_0 and a_2. An indispensable feature of any xc approximation within DFT is its ability to predict the properties of unknown materials or known materials under novel conditions; any free parameters must be internally determinable. As we now show, the Proca parameters have precisely this feature. We found the term a_0 to be material independent, but material class dependent: it is fixed to 0.2 for the case of strongly bound excitons and -0.2 for the case of weakly bound excitons. The results of our fit for a_2 are shown in Figs. 2(k)–2(l), revealing that this parameter depends linearly on the band gap. This linear form represents a universal relation between a calculable theoretical quantity—the gap—and the value of a_2 that yields accurate treatment of the excitonic response, guaranteeing a robust internally determinable scheme for the unknown parameters and hence a *bona fide* universal procedural functional. This parametrization is robust to the replacement of the local density approximation for xc (LDA) gap by its experimental value, as shown in the Supplemental Material [33]. More importantly, replacement of the LDA $v_{\rm xc}$ by that of a different approximation, for example the generalized gradient approximation (GGA), has a negligible impact on our results (this is also shown in the Supplemental Material [33]), reflecting the fact that excitonic physics in periodic solids is governed by $\mathbf{A}_{\rm xc}$ and not $v_{\rm xc}$. We would note that caution must be required for extended solids whose gap places the material intermediately between strongly bound and weakly bound excitonic physics.

One can also compare the natural length scale of the functional $\lambda = \sqrt{a_2/a_0}$ with the average excitonic Bohr radius. This comparison is plotted in Fig. 3. We find a linear relationship between λ and the exciton Bohr radius with the exception of GaAs, which is an outlier. This is evidence that the parameters a_0 and a_2 define both a current coupling strength as well as a screening length.

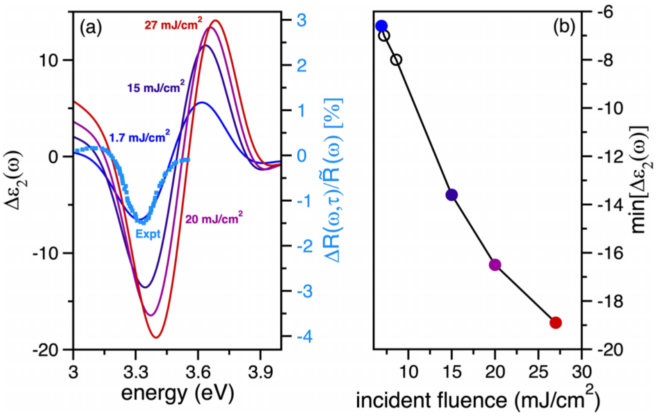

FIG. 4. For bulk Si, (a) the variation of change in the imaginary part of the dielectric tensor due to laser pumping $\Delta\varepsilon_2(\omega)$ as a function of photon energy (in eV), shown for different values of incident pump fluence (in mJ/cm^2) calculated using the KSP procedural functional. (b) The minimum value of $\Delta\varepsilon_2(\omega)$ as a function of incident fluence. Also shown are the experimental results [50] for the percentage change in reflectance upon low fluence laser pumping.

Excitons under strong pump laser conditions. To study strong laser-pumped excitons, we proceed by pumping bulk Si with short laser pulses (duration 12 fs) of varying fluence, three to four orders of magnitude larger than the probe pulse fluence. The system is again probed 50 fs after pumping. The change in absorption for Si is shown in Fig. 4(a), revealing a bleaching effect (decrease in absorption) between 3.3 and 3.6 eV and the appearance of side bands (i.e., increased absorption) above and below the bleached excitonic response. These features are in line with experiments on Si [50]—data also shown in Fig. 4(a)—that report bleaching between 3.3 and 3.5 eV and the appearance of side bands. Similar physics has also been reported in laser-pumped excitons in two-dimensional materials [5–7,51–55]. While we cannot directly compare the calculated amplitude with the experimental data, which is the percentage change in reflectivity, if we track the minimum of the $\Delta\varepsilon$ between 3 and 3.5 eV [see Fig. 4(b)], we find an initial linear behavior, exactly as in experiment [50]. This behavior deviates from linearity in a very strong-field regime.

The exchange-correlation vector potential evidently does not alter the ground state of the material, and hence the ground-state gap of the system is not affected by this formalism. The transient optical gap, however, which will not change in the limit of weak-field pumping, does change upon strong-field pumping and contributes, together with transient changes in screening, towards the shift of the excitonic peak in the energy range 3.3–3.6 eV. That two internally determinable parameters—a_0 and a_2—can capture both the excitons in the weak-field regime as well as the physics of exciton peak bleaching under strong-field pumping represents a striking demonstration of the power of the KSP procedural functional.

Discussion. We have presented a procedural functional KSP scheme that we have shown (i) has all parameters internally determinable due to a universal relation between the Proca mass and the band gap, (ii) possesses memory of the dynamics, and (iii) captures key features of excitonic physics both in the weak as well as in the strong laser-pumping regimes. The calculated response under weak laser pumping exhibits excellent agreement with experimental linear-response spectra for a wide class of materials, while for Si we have shown the KSP scheme captures key features of strong laser-pumped excitons (bleaching and the appearance of excitonic side bands).

In addition to this utility for the purely electronic system, the simultaneous time propagation of Kohn-Sham and Proca equations renders it easy to include additional degrees of freedom. Our approach thus both solves a crucial problem of TD-DFT—the ability to treat excitonic physics both in weak pumping as well as in the highly nonequilibrium strong pumping time-dependent case—but also opens rich new possibilities for the coupling of excitons to quasiparticles such as phonons and magnons, under laser-pump conditions.

Acknowledgments. S. Sharma, J.K.D., and D.G. would like to thank the DFG for funding through Project ID No. 328545488 TRR227 (project A04). S. Sharma and S. Shallcross are thankful for funding through the Leibniz Professorin Program (Grant No. SAW P118/2021).

[1] I. Zutić, J. Fabian, and S. D. Sarma, Spintronics: Fundamentals and applications, Rev. Mod. Phys. **76**, 323 (2004).
[2] J. R. Schaibley, H. Yu, G. Clark, P. Rivera, J. S. Ross, K. L. Seyler, W. Yao, and X. Xu, Valleytronics in 2D materials, Nat. Rev. Mater. **1**, 16055 (2016).
[3] A. Melnikov, I. Razdolski, T. O. Wehling, E. T. Papaioannou, V. Roddatis, P. Fumagalli, O. Aktsipetrov, A. I. Lichtenstein, and U. Bovensiepen, Ultrafast transport of laser-excited spin-polarized carriers in Au/Fe/MgO (001), Phys. Rev. Lett. **107**, 076601 (2011).
[4] S.-Y. Chen, T. Goldstein, J. Tong, T. Taniguchi, K. Watanabe, and J. Yan, Superior valley polarization and coherence of 2*s* excitons in monolayer WSe_2, Phys. Rev. Lett. **120**, 046402 (2018).
[5] E. J. Sie, A. Steinhoff, C. Gies, C. H. Lui, Q. Ma, M. Rosner, G. Schönhoff, F. Jahnke, T. O. Wehling, Y.-H. Lee *et al.*, Observation of exciton redshift-blueshift crossover in monolayer WS_2, Nano Lett. **17**, 4210 (2017).
[6] H. Ouyang, H. Chen, Y. Tang, J. Zhang, C. Zhang, B. Zhang, X. Cheng, and T. Jiang, All-optical dynamic tuning of local excitonic emission of monolayer MoS_2 by integration with $Ge_2Sb_2Te_5$, Nanophotonics **9**, 2351 (2020).
[7] Y. Kobayashi, C. Heide, A. C. Johnson, V. Tiwari, F. Liu, D. A. Reis, T. F. Heinz, and S. Ghimire, Floquet engineering of strongly driven excitons in monolayer tungsten disulfide, Nat. Phys. **19**, 171 (2023).
[8] E. Runge and E. K. U. Gross, Density-functional theory for time-dependent systems, Phys. Rev. Lett. **52**, 997 (1984).
[9] K. Krieger, J. K. Dewhurst, P. Elliott, S. Sharma, and E. K. U. Gross, Laser-induced demagnetization at ultrashort time scales: Predictions of TDDFT, J. Chem. Theory Comput. **11**, 4870 (2015).

[10] J. K. Dewhurst, P. Elliott, S. Shallcross, E. K. Gross, and S. Sharma, Laser-induced intersite spin transfer, Nano Lett. **18**, 1842 (2018).

[11] F. Siegrist, J. A. Gessner, M. Ossiander, C. Denker, Y. P. Chang, M. C. Schroder, A. Guggenmos, Y. Cui, J. Walowski, U. Martens, J. K. Dewhurst, U. Kleineberg, M. Münzenberg, S. Sharma, and M. Schultze, Light-wave dynamic control of magnetism, Nature (London) **571**, 240 (2019).

[12] S. Sharma, P. Elliott, and S. Shallcross, THz induced giant spin and valley currents, Sci. Adv. **9**, eadf3673 (2023).

[13] S. Sharma, P. Elliott, and S. Shallcross, Valley control by linearly polarized laser pulses: Example of WSe_2, Optica **9**, 947 (2022).

[14] M. Hofherr, S. Häuser, J. Dewhurst, P. Tengdin, S. Sakshath, H. Nembach, S. Weber, J. Shaw, T. J. Silva, H. Kapteyn *et al.*, Ultrafast optically induced spin transfer in ferromagnetic alloys, Sci. Adv. **6**, eaay8717 (2020).

[15] M. Schultze, K. Ramasesha, C. Pemmaraju, S. Sato, D. Whitmore, A. Gandman, J. S. Prell, L. Borja, D. Prendergast, K. Yabana *et al.*, Attosecond band-gap dynamics in silicon, Science **346**, 1348 (2014).

[16] R. Bertoni, C. W. Nicholson, L. Waldecker, H. Hübener, C. Monney, U. De Giovannini, M. Puppin, M. Hoesch, E. Springate, R. T. Chapman, C. Cacho, M. Wolf, A. Rubio, and R. Ernstorfer, Generation and evolution of spin-, valley-, and layer-polarized excited carriers in inversion-symmetric WSe_2, Phys. Rev. Lett. **117**, 277201 (2016).

[17] F. Sottile, V. Olevano, and L. Reining, Parameter-free calculation of response functions in time-dependent density-functional theory, Phys. Rev. Lett. **91**, 056402 (2003).

[18] L. Reining, V. Olevano, A. Rubio, and G. Onida, Excitonic effects in solids described by time-dependent density-functional theory, Phys. Rev. Lett. **88**, 066404 (2002).

[19] S. Botti, F. Sottile, N. Vast, V. Olevano, L. Reining, H.-C. Weissker, A. Rubio, G. Onida, R. Del Sole, and R. W. Godby, Long-range contribution to the exchange-correlation kernel of time-dependent density functional theory, Phys. Rev. B **69**, 155112 (2004).

[20] S. Sharma, J. K. Dewhurst, A. Sanna, and E. K. U. Gross, Bootstrap approximation for the exchange-correlation kernel of time-dependent density-functional theory, Phys. Rev. Lett. **107**, 186401 (2011).

[21] G. Onida, L. Reining, and A. Rubio, Electronic excitations: Density-functional versus many-body Green's-function approaches, Rev. Mod. Phys. **74**, 601 (2002).

[22] P. Ghosez, X. Gonze, and R. W. Godby, Long-wavelength behavior of the exchange-correlation kernel in the Kohn-Sham theory of periodic systems, Phys. Rev. B **56**, 12811 (1997).

[23] S. Sharma, J. K. Dewhurst, and E. K. U. Gross, Optical response of extended systems using time-dependent density functional theory, *First principles approaches to spectroscopic properties of complex materials*, edited by C. Di Valentin, S. Botti, and M. Cococcioni (Springer, Berlin, Heidelberg, 2014), pp. 235–257.

[24] G. Vignale and M. Rasolt, Current-and spin-density-functional theory for inhomogeneous electronic systems in strong magnetic fields, Phys. Rev. B **37**, 10685 (1988).

[25] P. Romaniello and P. L. de Boeij, Time-dependent current-density-functional theory for the metallic response of solids, Phys. Rev. B **71**, 155108 (2005).

[26] J. Sun, C.-W. Lee, A. Kononov, A. Schleife, and C. A. Ullrich, Real-time exciton dynamics with time-dependent density-functional theory, Phys. Rev. Lett. **127**, 077401 (2021).

[27] K. Yabana, T. Sugiyama, Y. Shinohara, T. Otobe, and G. F. Bertsch, Time-dependent density functional theory for strong electromagnetic fields in crystalline solids, Phys. Rev. B **85**, 045134 (2012).

[28] K. Yabana, T. Nakatsukasa, J.-I. Iwata, and G. Bertsch, Real-time, real-space implementation of the linear response time-dependent density-functional theory, Physica Status Solidi (B) **243**, 1121 (2006).

[29] K. Yabana and G. F. Bertsch, Time-dependent local-density approximation in real time, Phys. Rev. B **54**, 4484 (1996).

[30] D. J. Singh, *Planewaves Pseudopotentials and the LAPW Method* (Kluwer Academic, Boston, 1994).

[31] J. K. Dewhurst, S. Sharma *et al.*, elk.sourceforge.net.

[32] J. K. Dewhurst, K. Krieger, S. Sharma, and E. K. U. Gross, An efficient algorithm for time propagation as applied to linearized augmented plane wave method, Comput. Phys. Commun. **209**, 92 (2016).

[33] See Supplemental Material at http://link.aps.org/supplemental/10.1103/PhysRevB.111.L060302 for the table of the values of a_0 and a_2 for all studied materials. Results for Si and LiF obtained using the GGA functional and the effect of local fields are also presented. LiCl data are shown in a larger energy window.

[34] D. Roessler and W. Walker, Optical constants of magnesium oxide and lithium fluoride in the far ultraviolet, JOSA **57**, 835 (1967).

[35] V. Saile, M. Skibowski, W. Steinmann, P. Gürtler, E. Koch, and A. Kozevnikov, Observation of surface excitons in rare-gas solids, Phys. Rev. Lett. **37**, 305 (1976).

[36] G. Baldini, Ultraviolet absorption of solid argon, krypton, and xenon, Phys. Rev. **128**, 1562 (1962).

[37] R. Knox and N. Inchauspé, Exciton states in ionic crystals, Phys. Rev. **116**, 1093 (1959).

[38] P. Lautenschlager, M. Garriga, L. Vina, and M. Cardona, Temperature dependence of the dielectric function and interband critical points in silicon, Phys. Rev. B **36**, 4821 (1987).

[39] P. Lautenschlager, M. Garriga, S. Logothetidis, and M. Cardona, Interband critical points of GaAs and their temperature dependence, Phys. Rev. B **35**, 9174 (1987).

[40] M. Garriga, M. Kelly, and K. Ploog, Temperature dependence of the dielectric function and interband critical points of AlAs obtained on an MBe grown layer, Thin Solid Films **233**, 122 (1993).

[41] H. Phillip and E. Taft, Kramers-Kronig analysis of reflectance data for diamond, Phys. Rev. **136**, A1445 (1964).

[42] V. Cimalla, V. Lebedev, U. Kaiser, R. Goldhahn, C. Foerster, J. Pezoldt, and O. Ambacher, Polytype control and properties of ALn on silicon, Phys. Status Solidi (C) **2**, 2199 (2005).

[43] J. Sanmartín-Matalobos, P. Bermejo-Barrera, M. Aboal-Somoza, M. Fondo, A. M. García-Deibe, J. Corredoira-Vázquez, and Y. Alves-Iglesias, Semiconductor quantum dots as target analytes: Properties, surface chemistry and detection, Nanomaterials **12**, 2501 (2022).

[44] P. Puschnig and C. Ambrosch-Draxl, Optical absorption spectra of semiconductors and insulators including electron-hole correlations: An *ab initio* study within the LAPW method, Phys. Rev. B **66**, 165105 (2002).

[45] M. Shahrokhi and B. Mortazavi, Lithium halide monolayer sheets: First-principles many-body calculations, Comput. Mater. Sci. **143**, 103 (2018).
[46] H. Okushi, H. Watanabe, and S. Kanno, Characteristics of excitonic emission in diamond, Phys. Status Solidi (A) **202**, 2051 (2005).
[47] F. Bechstedt, K. Seino, P. H. Hahn, and W. G. Schmidt, Quasiparticle bands and optical spectra of highly ionic crystals: AlN and NaCl, Phys. Rev. B **72**, 245114 (2005).
[48] F. Sottile, M. Marsili, V. Olevano, and L. Reining, Efficient *ab initio* calculations of bound and continuum excitons in the absorption spectra of semiconductors and insulators, Phys. Rev. B **76**, 161103(R) (2007).
[49] A. Marini, R. Del Sole, and A. Rubio, Bound excitons in time-dependent density-functional theory: Optical and energy-loss spectra, Phys. Rev. Lett. **91**, 256402 (2003).
[50] D. Sangalli, S. Dal Conte, C. Manzoni, G. Cerullo, and A. Marini, Nonequilibrium optical properties in semiconductors from first principles: A combined theoretical and experimental study of bulk silicon, Phys. Rev. B **93**, 195205 (2016).
[51] Z. Nie, R. Long, L. Sun, C.-C. Huang, J. Zhang, Q. Xiong, D. W. Hewak, Z. Shen, O. V. Prezhdo, and Z.-H. Loh, Ultrafast carrier thermalization and cooling dynamics in few-layer MoS_2, ACS Nano **8**, 10931 (2014).
[52] C. Mai, A. Barrette, Y. Yu, Y. G. Semenov, K. W. Kim, L. Cao, and K. Gundogdu, Many-body effects in valleytronics: Direct measurement of valley lifetimes in single-layer MoS_2, Nano Lett. **14**, 202 (2014).
[53] V. Smejkal, F. Libisch, A. Molina-Sanchez, C. Trovatello, L. Wirtz, and A. Marini, Time-dependent screening explains the ultrafast excitonic signal rise in 2D semiconductors, ACS Nano **15**, 1179 (2021).
[54] M. Lucchini, S. A. Sato, G. D. Lucarelli, B. Moio, G. Inzani, R. Borrego-Varillas, F. Frassetto, L. Poletto, H. Hübener, U. De Giovannini *et al.*, Unravelling the intertwined atomic and bulk nature of localised excitons by attosecond spectroscopy, Nat. Commun. **12**, 1021 (2021).
[55] S. Sim, J. Park, J.-G. Song, C. In, Y.-S. Lee, H. Kim, and H. Choi, Exciton dynamics in atomically thin MoS_2: Interexcitonic interaction and broadening kinetics, Phys. Rev. B **88**, 075434 (2013).